

Mussel-Inspired Plasmonic Nanohybrids for Light Harvesting

Minah Lee, Jong Uk Kim, Joon Seok Lee, Byung Il Lee, Jonghwa Shin,*
and Chan Beum Park*

Solar energy conversion begins with light absorption by photosensitizers, whereby the electric excitation is transferred to a specific electron acceptor. In green plants, for example, protein complexes tightly bound with highly concentrated chromophores in an elaborate architecture ensure strong light absorption and effective energy transport to reaction centers during photosynthesis.^[1] Inspired by natural photosynthesis, amplifying light absorption has been regarded as one of key challenges in achieving maximal efficiency in artificial photosynthetic systems through solar energy harvesting.^[2] Coupling such photocatalytic systems with metallic nanostructures that exhibit strong localized surface plasmon resonance (LSPR) is considered to be a promising strategy.^[3,4] The intense, local electric fields induced by collective electron oscillation in metals upon resonant excitation can enhance photoexcitation of adjacent photoactive species, such as molecular chromophores or semiconductors.^[5,6] Recent studies have exploited LSPR to efficiently harvest and utilize solar energy for applications in photovoltaics to generate electricity,^[7–9] and in chemical processes to obtain energetically useful or chemically valuable products.^[10–17]

The primary issue in achieving plasmon-enhanced light harvesting lies in the precise architecture of metal nanostructures and photosensitizers, because different kinds of energy transfer interactions can predominate depending on their geometries.^[18] Over the last few decades, there have been significant advances in fabrication routes for metallic nanostructures, which include focused ion beam milling, electron-beam lithography, and wet chemical synthesis.^[19–21] However, obstacles such as low throughput and high cost due to serial writing under high vacuum in case of top-down approaches and the need for extra schemes in the arrangement and adhesion of colloidal nanoparticles (NPs) on substrates limit their applicability to artificial light harvesting systems. Furthermore, synthetic strategies for precise incorporation of photosensitizers to such fine metal nanostructures, which often occurs in a random manner,^[22,23] have yet to be established for the development of complex plasmon-enhanced light harvesting assemblies.^[24] Therefore, inexpensive, scalable, and

accurate synthetic strategies for assembling plasmonic metal nanostructures, as well as strategies for hybridizing them with targeted photocatalytic systems, are in high demand to realize practical applications of plasmonics in solar-to-energy conversion.

Here we present a simple and versatile approach for the construction of plasmonic metal/photosensitizer core-shell nanohybrids for efficient light harvesting by adopting multi-purpose polydopamine (PDA) nanolayers inspired by mussel adhesion. As a mimicry of mussel adhesive proteins, PDA coating can be applied to a wide variety of material surfaces^[25] and allows facile synthesis of various functional nanostructures.^[26–28] In our plasmonic core-shell assembly (Figure 1a), PDA coating plays multiple roles: (1) a reducing agent for the synthesis of metal NPs, (2) a scaffold for the encapsulation of photosensitizing dye molecules, and (3) an adhesive layer between the nanohybrid and the substrate. In contrast to nanolithography processes, the entire synthetic procedure can be handled in an aqueous solution under mild conditions and requires no intricate equipment, which confers advantages in large-scale production. Also, by virtue of the remarkable adhesive versatility of PDA coating, this approach can be applied to the development of elaborate core-shell nanostructures regardless of material type and morphology of substrates. We found that the resulting plasmonic nanohybrids exhibit strongly enhanced photocatalytic activity during visible light-induced artificial photosynthesis as a result of amplified light absorption by molecular photosensitizers through LSPR from the plasmonic metal NPs. We expect that a diverse range of metal core (e.g., gold and silver) and dye molecule combinations are possible through the use of our strategy to facilitate the synthesis of assorted sets of nanohybrids with desired optical properties, allowing design flexibility in solar energy conversion applications.

The synthesis of plasmonic nanohybrids with metal cores surrounded by photosensitizer-encapsulating shells is accomplished through a facile, three-step incubation process, as depicted in Figure S1. The first step is to form the PDA layer on a substrate through oxidative polymerization of dopamine using a simple immersion process. Plasmonic metal NPs are then deposited on the PDA-coated substrate in a metal precursor solution by utilizing the reducing capability of catecholic moieties in PDA. Finally, the secondary PDA coating is applied to encapsulate photosensitizing molecules around the plasmonic metal cores. While both gold and silver NPs were tested as plasmonic noble metals in this work, Au NPs were mainly utilized for photocatalytic reactions because of their higher thermal, chemical, and photochemical stabilities compared to Ag NPs. While different types of photosensitizing molecules

M. Lee, J. U. Kim, Dr. J. S. Lee, B. I. Lee, Prof. J. Shin,
Prof. C. B. Park
Department of Materials Science and Engineering
KAIST Institute for NanoCentury
KAIST, Daejeon 305–701, Republic of Korea
E-mail: qubit@kaist.ac.kr; parkcb@kaist.ac.kr



DOI: 10.1002/adma.201305766

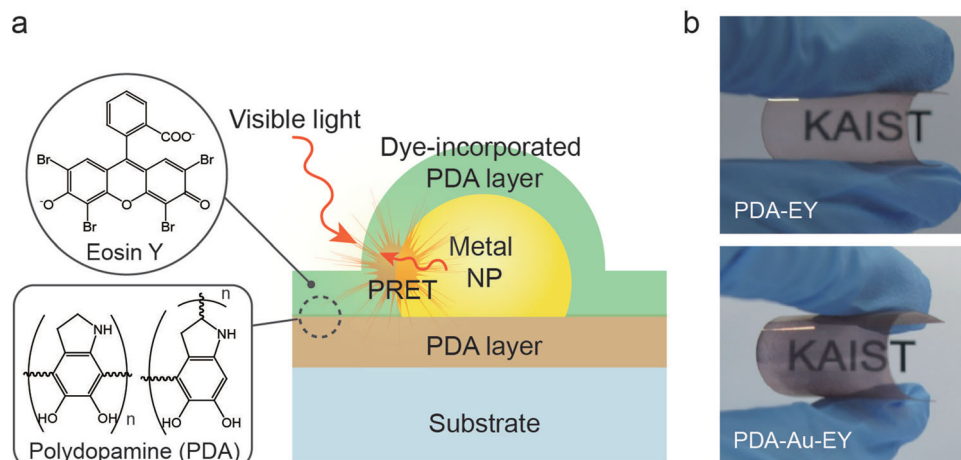


Figure 1. a) Schematic illustration of mussel-inspired plasmonic nanohybrid for light harvesting. PDA coating enables formation of core-shell nanostructures integrated with metal NPs and photosensitizers, irrespective of the material type and morphology of substrates. b) Photographs of nanohybrid films formed on flexible PET substrates. Eosin Y was coupled with Au NPs as a model system of plasmonic nanohybrid for artificial photosynthesis.

can be incorporated in the PDA ad-layer (see Figure S2), we used eosin Y (EY) as a model photosensitizer for plasmon-enhanced solar energy conversion. EY, one of the xanthenes dyes, has been identified as an excellent light harvester for biocatalyzed artificial photosynthesis.^[29,30] The photographs in Figure 1b show red translucent films of nanohybrids formed on a flexible polyester (PET) substrate, where PDA-EY indicates a film consisting of a primary PDA layer and a secondary PDA layer that encapsulates EY, and PDA-Au-EY corresponds to a sample having the primary PDA layer, plasmonic Au NP cores, and the secondary PDA layer with EY.

We performed mussel-inspired nanohybrid synthesis on three different substrates (slide glasses, flexible PET films, and silica beads [900 nm in diameter]) to demonstrate the material- and morphology-independency of our approach. The SEM images in Figure 2a (left) show that plasmonic Au NPs were successfully formed on each PDA-coated substrate through incubation in a gold chloride solution. The Au NPs exhibited a size distribution ranging from 30 to 100 nm with the average size being ~70 nm (Figures S3, S4). After the secondary PDA coating accompanying EY encapsulation, the EY shell layer surrounding Au NPs was observed. The clear contrast between bright inner cores—corresponding to Au NPs—and pale PDA sheaths of approximately 20 nm in thickness was easily observable, indicating the existence of well-defined core/shell nanostructures. This hybrid nanostructure of metal core/dye shell ensures that a significant portion of dye molecules should be located in the plasmonic enhancement region.

We analyzed PDA-only, PDA-Au, PDA-EY, and PDA-Au-EY films assembled on glass substrates using XPS spectroscopy to examine the composition of plasmonic nanohybrids (Figure 2b). All of the films exhibited characteristic peaks at C 1s, N 1s, and O 1s that originated from PDA. The PDA-Au film clearly shows additional peaks located at the binding energy of 84.2 and 87.8 eV corresponding to Au 4f, which suggests successful formation of Au NPs. In the PDA-EY and PDA-Au-EY spectra, the characteristic peaks of Br 3p at 190 eV and Br 3d at 69.5 eV confirm the existence of EY in the samples. Note that the

substantial decrease in the characteristic peaks of Au 4f after the secondary PDA-coating in the PDA-Au-EY sample indicates that most Au NPs are enclosed by the PDA shell. The XRD pattern of PDA-Au matched well with the database of metallic Au (JCPDS No. 65–8601), which further confirms the formation of crystalline Au NPs on the surface of the PDA-coated substrate (Figure S5). The broad peaks in the range of 20–30° in the PDA-only and PDA-Au films are due to the amorphous nature of PDA. In addition, our approach enabled the synthesis of plasmonic nanohybrids by employing Ag NPs as metal cores (Figure S6).

We investigated the LSPR of Au NPs and their interaction with EY using UV-Vis absorption spectroscopy by comparing the absorbance spectra of different hybrid samples (Figure 3a). The characteristic absorption peak of EY at 538 nm is easily identifiable in the PDA-EY film when compared to the PDA-only film. With regards to PDA-Au-EY nanohybrids, two neighboring peaks appear in the spectrum, which originate from the presence of EY and Au NPs. Compared to the PDA-EY film, the Au NP-incorporating sample (i.e., PDA-Au-EY) exhibits significantly enhanced absorption intensity at 538 nm. The additional, broad peak at near 600 nm is attributed to the LSPR peaks of Au NPs that have been inhomogeneously broadened due to the diameter and shape variations of Au NPs. Also, the peak position is red-shifted compared to that of bare Au NPs formed on a PDA layer (i.e., PDA-Au), which is an expected outcome of the increased effective refractive index of the surrounding medium.

We further investigated the optical properties of plasmonic nanohybrids using numerical electromagnetic simulation to confirm electromagnetic field enhancement by Au NPs and to examine their effect on dye absorption. Finite difference time domain (FDTD) calculation governed by Maxwell's equation has been performed (see the Experimental Section for details), which is a highly accurate tool in the study of electromagnetic properties of complex nanostructures.^[31] As shown in Figure S7, the resulting spectra of calculated absorbance for different hybrid films (e.g., PDA-only, PDA-EY, PDA-Au, and PDA-Au-EY films) were consistent with the experimental results in

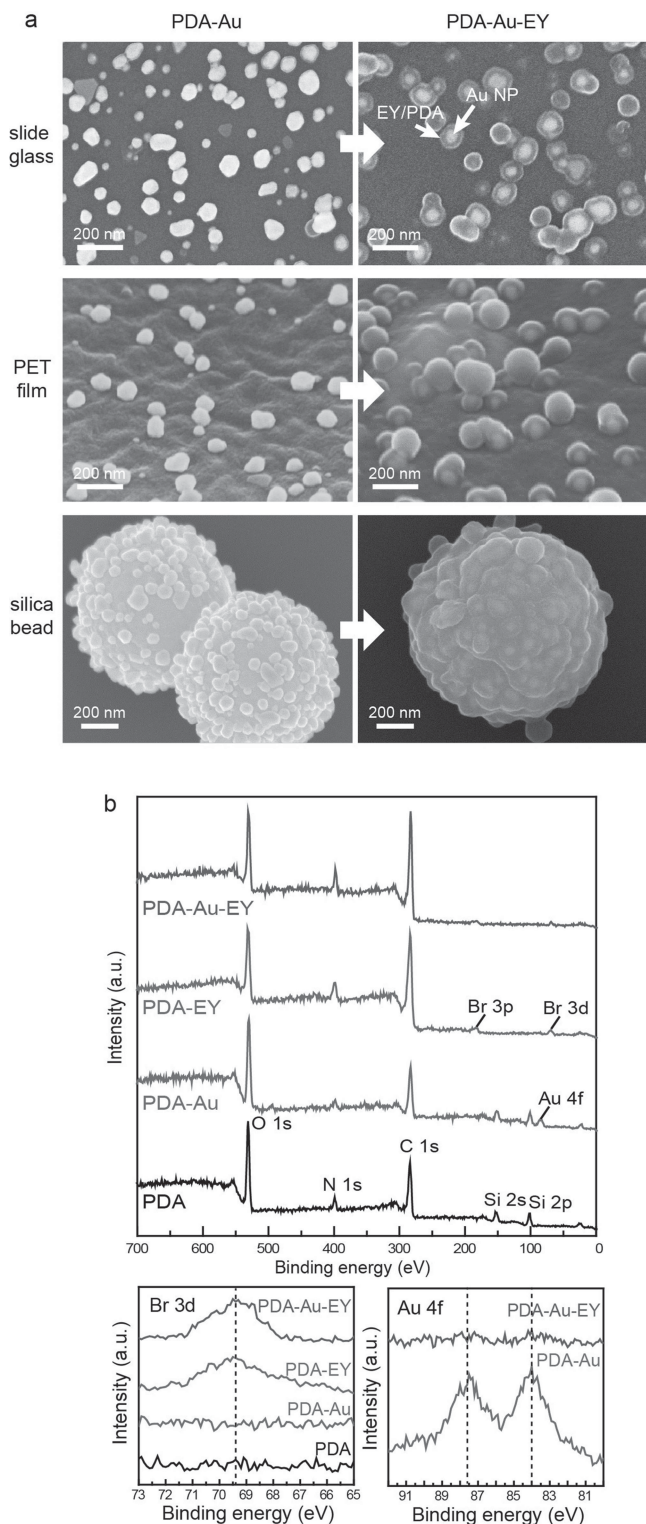


Figure 2. a) SEM images of plasmonic nanohybrids formed on slide glasses, PET films, and silica beads (900 nm), indicating general applicability of our strategy. Au NPs formed on PDA coated substrates (left) are confined by EY-incorporated shells after secondary PDA coating (right). b) XPS survey spectra (top), Br 3d XPS spectra (bottom, left), and Au 4f XPS spectra (bottom, right) of nanohybrids with different layers.

Figure 3a; the LSPR peak of Au NPs overlapped with the EY absorption peak. In the numerical investigation of PDA-Au-EY film, the absorption due to each component of layer could be separately calculated using local electric field distributions. According to the results shown in Figure 3b, the most intense absorption occurred in the top EY layer and the absorption intensity of EY in the PDA-Au-EY film increased markedly in comparison with the absorption of EY in the PDA-EY film not having Au NPs, although non-negligible absorption of Au NPs did exist. Figure 3c illustrates electric field distribution at the absorption band of EY, which demonstrates the strong field enhancement induced by the Au NPs due to the LSPR. In the PDA-Au-EY film, EY molecules in the PDA shell covering the Au core are located in the plasmonic field enhancement region; thus, the enhanced light absorption by EY is attributed to the field distribution. The field enhancement by the LSPR of Au NPs was also supported by an analysis using surface-enhanced resonance Raman spectroscopy (SERS). Figure 3d shows the SERS spectra of PDA, PDA-EY, and PDA-Au-EY films, which were acquired using an excitation of 514 nm. Significant enhancement in the EY's Raman peaks at 1621, 1506, 1341, 1281, and 1179 cm^{-1} was observed in the sample with Au NPs (i.e., PDA-Au-EY film) in comparison with the PDA-EY film, which originate from typical vibrational modes in the xanthenone and benzene rings of the EY molecule.^[32] The amplified SERS signal clearly evidences the enhanced electromagnetic field by Au NPs in the PDA-Au-EY film.

We employed the plasmonic nanohybrid assemblies for biocatalyzed artificial photosynthesis, which facilitates visible light-induced recycling of nicotinamide cofactor (NADH) and redox enzymatic chemical synthesis to mimic natural photosynthesis.^[33–35] In green plants, photosynthesis occurs through photo-regeneration of nicotinamide cofactor and their consumption in the Calvin cycle, converting solar energy into chemical energy.^[36–38] As illustrated in Figure 4a, during the artificial photosynthetic reaction using PDA-Au-EY, photo-excited electrons in EY are transferred to an electron mediator ($M = [Cp^*Rh(bpy)H_2O]^{2+}$, $Cp^* = C_5Me_5$, $bpy = 2,2'$ -bipyridine) under visible light illumination ($\lambda > 420$ nm), which facilitates the regeneration of NADH in an enzymatically-active form so that NADH-dependent oxidoreductase (e.g., L-glutamate dehydrogenase, GDH) can consume NADH to produce L-glutamate from α -ketoglutarate. As demonstrated earlier, EY in the core-shell conformation of PDA-Au-EY film should experience the enhanced local electromagnetic field near the Au cores upon visible-light illumination, whereby light absorption and photoelectron generation in EY can be boosted. Furthermore, the secondary PDA-coating encapsulating EY can electronically and chemically insulate the metal core from direct contact with the photocatalysts and redox mediators^[39–41] to prevent charge recombination and metal corrosion.^[7,9] Figure 4b shows photoregeneration yields of NADH from NAD^+ under visible light with different nanohybrid films (PDA-Au, PDA-EY, and PDA-Au-EY). A detailed experimental set-up is described in the Experimental Section. Significant enhancement in the photocatalytic activity of EY due to the incorporation of plasmonic Au NPs was evident; PDA-Au-EY film resulted in a NADH photoregeneration yield of 14.7% while PDA-EY film regenerated only 2.1% of NAD^+ to NADH. Note

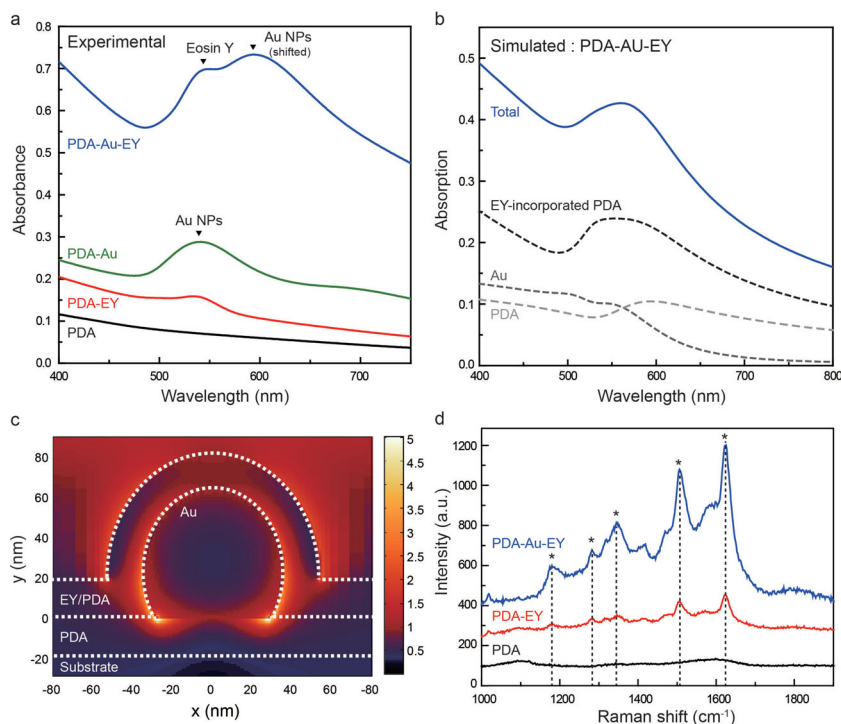


Figure 3. a) Absorbance of nanostructures with different layers. b) Simulated total absorption of PDA-Au-EY and the individual absorption spectra of each material from FDTD methods. c) Distributions of the electric field intensity around Au NPs (70 nm) with the EY-incorporated PDA shell (20 nm). d) Comparison of the SERS spectra for PDA, PDA-EY, and PDA-Au-EY films.

that no regeneration of NADH was observed with PDA-Au film under the same reaction conditions. We calculated the plasmon-enhancement factor to be five using the NADH photoregeneration yields of PDA-EY and PDA-Au-EY. Because the surface areas for both samples differed depending on the presence of Au NPs, the augmentation factor of 1.4 for EY coverage in the PDA-Au-EY sample has been taken into account for the calculation. The PDA-Au-EY film was completely recovered without any dye leaching or plasmonic band change for Au NPs after the photocatalytic reaction (Figure S8). The plasmon-derived enhancement was also demonstrated in the enzymatic photosynthesis of L-glutamate by GDH coupled with the photochemical NADH regeneration. As shown in the inset of Figure 4b, PDA-Au-EY produced 2 mM of L-glutamate while PDA-EY produced less than 0.1 mM of L-glutamate from 10 mM of α -ketoglutarate.

The photocatalysis of NADH regeneration using plasmonic nanostructures was further studied by introducing a spacing layer between the Au core and the EY layer to observe distance dependence of the plasmon enhancement, providing additional evidence for LSPR from Au NPs. The placement of the spacing layer was achieved by applying another PDA coating through incubation of the PDA-Au film in a dopamine-only solution prior to the formation of the EY layer. PDA spacing layers with three different thicknesses (of 2.5, 11, and 22 nm) were introduced by controlling the duration of the immersion of PDA-Au film for 20 min, 3 hrs, and 6 hrs, respectively (Figure S9). The ratio of NADH regeneration yields by PDA-Au-EY is plotted against the spacing thickness in Figure 4c.

Note that the result of plasmonic enhancement during NADH regeneration reflected comprehensive interactions of all the dyes in the 20 nm-thick PDA layers, where the distances between Au NPs and dyes were varied from 0 to 20 nm in addition to the thickness of the spacing layers. The photosynthetic yields of the nanostructures with the spacing layers were always lower than that of the PDA-Au-EY film without the spacing layer, which gradually decreased as the distance (i.e., the spacing layer thickness) between Au and EY increased. The distance dependence confirms that the enhancement in the photosynthetic reaction is strongly dependent on the LSPR produced by Au NPs, because LSPR induces higher concentration of light in closer proximity to metal NPs.^[42,43] We further validated the distance dependence of the field enhancement by Au NPs using FDTD calculation (Figure S10). Additional predictable interactions between dye molecules and plasmonic metal NPs in the nanostructure, such as non-radiative energy transfer from dye to metal that occurs at short distances,^[18] or charge recombination due to direct contact of metal and dye molecules,^[9] appear to be insignificant compared to the absorption enhancement since PDA-Au-EY without the spacing

layer always resulted in higher regeneration yields than the nanostructures with PDA spacings. Therefore, our results show that the core-shell structure of the PDA-Au-EY nanostructures is suitable for plasmon-enhanced artificial photosynthesis and the field enhancement by the LSPR from Au NPs is critical for the enhanced photocatalytic efficiency of EY during NADH photoregeneration.

In summary, we created core-shell nanostructure assemblies for plasmon-enhanced light harvesting by employing multifunctional mussel-inspired PDA nanolayers as a reducing agent for plasmonic metal deposition, a scaffold for dye encapsulation, and an adhesive between nanostructure and substrate. Utilizing the remarkable adhesive versatility of PDA coating, we successfully synthesized elaborate, core-shell nanostructures on different substrates to demonstrate general applicability to materials irrespective of their chemical compositions or morphologies. The resulting plasmonic nanostructures, in which dye molecules are precisely located in the field enhancement region by the LSPR around the metal core, enabled plasmon-enhanced light absorption and charge carrier generation in the photosensitizing molecules. Upon visible-light illumination, the plasmonic metal NPs incorporated in the light harvesting assemblies significantly enhanced the photocatalytic activity by the molecular photosensitizer during biocatalyzed artificial photosynthesis. The mussel-inspired approach provides an effective and innovative platform to attain nanoscale architectures integrated with plasmonic metals and photocatalysts with desired optical properties for solar energy harvesting.

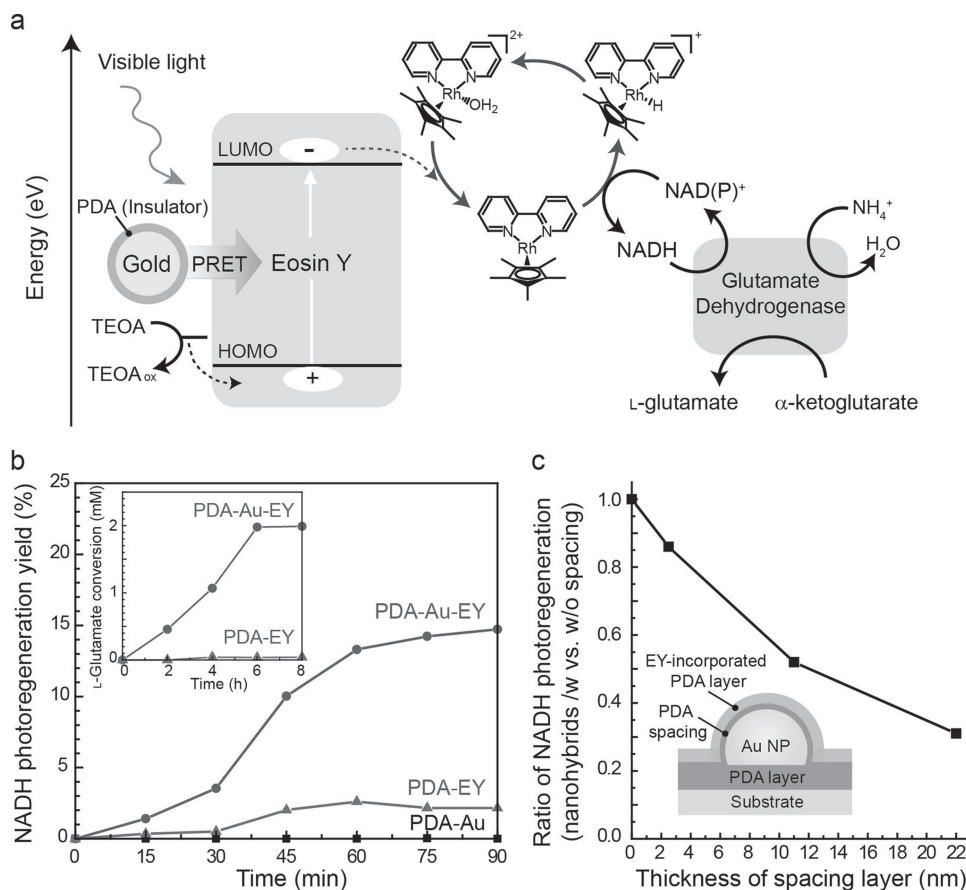


Figure 4. a) Energy level diagram of plasmon-enhanced biomimetic photosynthesis by PDA-Au-EY nano hybrids. b) Photoregeneration of NADH using PDA-Au, PDA-EY, and PDA-Au-EY nano hybrid films under visible light. The inset shows photoenzymatic synthesis of L-glutamate by GDH coupled with photoregeneration of NADH by nano hybrid films. c) Ratio of the NADH photoregeneration yield of PDA-Au-EY with PDA spacing to that of PDA-Au-EY without PDA spacing plotted against the thickness of the spacing layers.

Experimental Section

Materials: Dopamine hydrochloride, gold(III) chloride hydrate, silver nitrate, tris base, eosin Y (EY), phloxine B, tris(2,2'-bipyridyl) dichlororuthenium(II)hexahydrate ($\text{Ru}[\text{bpy}]_3$), triethanolamine (TEOA), NAD^+ , α -ketoglutarate, ammonium sulfate, and glutamate dehydrogenase (GDH) were purchased from Sigma-Aldrich (St. Louis, MO). $\text{Cu}(\text{II})$ tetrakis(4-sulfonatophenyl)porphyrin (TPPS) was purchased from Frontier Scientific (Logan, UT). Slide glasses and PET films were washed with ethanol and deionized water prior to nano hybrid synthesis. Silica beads were synthesized by the seeded growth method as described in the literature.^[44] $[\text{Cp}^*\text{Rh}(\text{bpy})\text{H}_2\text{O}]^{2+}$ was synthesized according to the previous study.^[29]

Mussel-Inspired Nano hybrid Synthesis: The synthesis of nano hybrid films was achieved on the substrates of different materials and morphologies through the same three-step incubation procedure. First, PDA coating was created by immersing the substrate into a dopamine solution (2 mg mL^{-1}) in Tris buffer (10 mM, pH 8.5). Then, the PDA-coated substrate was incubated in the metal precursor solution to induce reduction of plasmonic metal nanoparticles by catecholic moieties in PDA. 1 mM of gold chloride solution was used for Au NPs synthesis and 50 mM of silver nitrate solution was used for Ag NPs synthesis. Secondary PDA coating for dye encapsulation was followed by dipping the resulting sample into a dye (1 mg mL^{-1})/dopamine (2 mg mL^{-1}) solution in Tris buffer. All of the incubation steps were performed in a shaking incubator (JO Tech., Korea) at a shaking rate of 100 rpm for 16 hrs.

Characterization of Nano hybrids: The morphologies of nano hybrid films were observed using an S-4800 field emission scanning electron microscope (Hitachi High-technologies CO., Japan). The analysis of elements comprising the films was performed by X-Ray photoelectron spectroscopy (XPS) using a sigma probe spectrometer (Thermo VG Scientific Co., UK) equipped with a microfocusing monochromated X-ray source (90 W) under an ultrahigh vacuum condition ($\sim 10^{-10}$ Torr). Absorbance spectra of the samples were measured using a V/650 spectrophotometer (Jasco, Inc., Tokyo, Japan). The Raman spectra were obtained with a LabRAM UV-vis-NIR high-resolution dispersive Raman microscope (Horiba Jobin Yvon, France). The diffraction patterns of metal nanoparticles were measured using a D/MAX-2500 X-ray diffractometer (Rigaku Co., Japan).

FDTD Simulation: In order to calculate the optical properties of nano hybrid systems with FDTD simulations, complex permittivities of PDA and EY were first modeled. For PDA, the real part of the permittivity was exploited from the previous reported value.^[45] The transfer-matrix method was employed to retrieve the imaginary part of PDA from the experimental absorbance result. EY permittivity was calculated using a Lorentz model, $\epsilon_{\text{EY}} = \epsilon_{\text{PDA}} + \frac{\epsilon_{\text{Lorentz}} \cdot \omega_{\text{resonance}}^2}{\omega^2 - \omega_{\text{resonance}}^2 - i\Gamma\omega}$, where ϵ_{PDA} was a calculated value, $\epsilon_{\text{Lorentz}} = 0.03$, damping (Γ) = $3.5 \times 10^{14} \text{ s}^{-1}$, and $\omega_{\text{resonance}} = 3.5 \times 10^{15} \text{ s}^{-1}$ ($\lambda_{\text{resonance}} = 540 \text{ nm}$). For Au, an empirical result of Johnson and Christy was used.^[46] With these material parameters, numerical simulations were conducted using the finite-difference time-domain method. A mean size (70 nm) of Au NPs from the experiment was chosen to evaluate the local optical properties of nano hybrid films.

In this simulation, simulation volume was meshed into 1 nm resolution in the organic and metallic regions. Far removed from the organic and metallic regions, a larger mesh size was used to reduce computational load. Total simulation volume was $170 \times 220 \times 170 \text{ nm}^3$ and a plane wave source, propagating in y direction, was used. Periodic boundaries were employed in x- and z-direction and perfectly matched layers were adopted in y direction for termination. 3-dimensional and 2-dimensional monitors were used to collect electric field data for calculation of the field enhancement and absorption.

NADH Photoregeneration and Photoenzymatic Synthesis of L-Glutamate: For the photoregeneration of NADH, nanohybrid films formed on slide glasses were immersed in 3 mL of reaction medium in quartz cells and were kept in the dark with vigorous stirring for 30 minutes to ensure fully homogenized reactors before the photocatalytic reaction. The reaction medium was composed of NAD^+ (1 mM), $[\text{Cp}^*\text{Rh}(\text{bpy})\text{H}_2\text{O}]^{2+}$ (0.5 mM), and TEOA (15 w/v%) in a phosphate buffer (100 mM, pH 7.5). A xenon lamp (450 W) with a 420-nm cut-off filter was used as a light source. During light irradiation, the absorbance of the reaction medium at 340 nm was measured to estimate the concentration of photoregenerated NADH. The photoenzymatic synthesis of L-glutamate coupled with photoregeneration of NADH was performed using the same experimental set-up with the exception of the reaction medium. The reaction medium for L-glutamate conversion consisted of NAD^+ (1 mM), $[\text{Cp}^*\text{Rh}(\text{bpy})\text{H}_2\text{O}]^{2+}$ (0.5 mM), TEOA (15 w/v%), α -ketoglutarate (5 mM), $(\text{NH}_4)_2\text{SO}_4$ (100 mM), and GDH (40 U) in a phosphate buffer (100 mM, pH 7.5). The amount of L-glutamate during the photoenzymatic reaction was analyzed using liquid chromatography (LC-20A prominence, Shimadzu, Japan) equipped with an Inertsil C18 column (ODS-3V, length: 150 mm).

Supporting Information

Supporting Information is available from the Wiley Online Library or from the author.

Acknowledgements

This work was supported from the National Research Foundation (NRF) grants of the National Leading Research Laboratory (NRF-2013R1A2A1A05005468), the Intelligent Synthetic Biology Center of Global Frontier R&D Project (2011-0031957), the Converging Research Center (2010-50207), the NRF MSIP Project (No. 2008-0061893, NRF-2012M3A7B4035327), and the NRF R&D Joint Venture Program.

Received: November 21, 2013

Revised: January 27, 2014

Published online:

- [1] G. D. Scholes, G. R. Fleming, A. Olaya-Castro, R. van Grondelle, *Nat. Chem.* **2011**, *3*, 763.
- [2] A. A. Boghossian, M.-H. Ham, J. H. Choi, M. S. Strano, *Energy Environ. Sci.* **2011**, *4*, 3834.
- [3] S. Linic, P. Christopher, D. B. Ingram, *Nat. Mater.* **2011**, *10*, 911.
- [4] H. A. Atwater, A. Polman, *Nat. Mater.* **2010**, *9*, 205.
- [5] S. C. Warren, E. Thimsen, *Energ. Environ. Sci.* **2012**, *5*, 5133.
- [6] W. Hou, S. B. Cronin, *Adv. Funct. Mater.* **2013**, *23*, 1612.
- [7] J. Qi, X. Dang, P. T. Hammond, A. M. Belcher, *ACS Nano* **2011**, *5*, 7108.
- [8] A. P. Kulkarni, K. M. Noone, K. Munechika, S. R. Guyer, D. S. Ginger, *Nano Lett.* **2010**, *10*, 1501.
- [9] M. D. Brown, T. Suteewong, R. S. S. Kumar, V. D'Innocenzo, A. Petrozza, M. M. Lee, U. Wiesner, H. J. Snaith, *Nano Lett.* **2010**, *11*, 438.
- [10] S. Mubeen, J. Lee, N. Singh, S. Kramer, G. D. Stucky, M. Moskovits, *Nat. Nanotechnol.* **2013**, *8*, 247.
- [11] D. B. Ingram, S. Linic, *J. Am. Chem. Soc.* **2011**, *133*, 5202.
- [12] S. Mukherjee, F. Libisch, N. Large, O. Neumann, L. V. Brown, J. Cheng, J. B. Lassiter, E. A. Carter, P. Nordlander, N. J. Halas, *Nano Lett.* **2012**, *13*, 240.
- [13] Z. W. Seh, S. Liu, M. Low, S.-Y. Zhang, Z. Liu, A. Mlayah, M.-Y. Han, *Adv. Mater.* **2012**, *24*, 2310.
- [14] F. Wang, C. Li, H. Chen, R. Jiang, L.-D. Sun, Q. Li, J. Wang, J. C. Yu, C.-H. Yan, *J. Am. Chem. Soc.* **2013**, *135*, 5588.
- [15] A. Marimuthu, J. Zhang, S. Linic, *Science* **2013**, *339*, 1590.
- [16] K. Mori, M. Kawashima, M. Che, H. Yamashita, *Angew. Chem. Int. Ed.* **2010**, *49*, 8598.
- [17] E. Seo, J. Kim, Y. Hong, Y. S. Kim, D. Lee, B.-S. Kim, *J. Phys. Chem. C* **2013**, *117*, 11686.
- [18] H. Chen, T. Ming, L. Zhao, F. Wang, L.-D. Sun, J. Wang, C.-H. Yan, *Nano Today* **2010**, *5*, 494.
- [19] H. Duan, H. Hu, K. Kumar, Z. Shen, J. K. W. Yang, *ACS Nano* **2011**, *5*, 7593.
- [20] J. A. Fan, C. Wu, K. Bao, J. Bao, R. Bardhan, N. J. Halas, V. N. Manoharan, P. Nordlander, G. Shvets, F. Capasso, *Science* **2010**, *328*, 1135.
- [21] M. R. Jones, K. D. Osberg, R. J. Macfarlane, M. R. Langille, C. A. Mirkin, *Chem. Rev.* **2011**, *111*, 3736.
- [22] C.-W. Yen, S. C. Hayden, E. C. Dreaden, P. Szymanski, M. A. El-Sayed, *Nano Lett.* **2011**, *11*, 3821.
- [23] I. Kim, S. L. Bender, J. Hranisavljevic, L. M. Utschig, L. Huang, G. P. Wiederrecht, D. M. Tiede, *Nano Lett.* **2011**, *11*, 3091.
- [24] L. Novotny, N. van Hulst, *Nat. Photon.* **2011**, *5*, 83.
- [25] H. Lee, S. M. Dellatore, W. M. Miller, P. B. Messersmith, *Science* **2007**, *318*, 426.
- [26] J. Sedó, J. Saiz-Poseu, F. Busqué, D. Ruiz-Molina, *Adv. Mater.* **2013**, *25*, 653.
- [27] S. M. Kang, N. S. Hwang, J. Yeom, S. Y. Park, P. B. Messersmith, I. S. Choi, R. Langer, D. G. Anderson, H. Lee, *Adv. Funct. Mater.* **2012**, *22*, 2949.
- [28] J. Ryu, S. H. Ku, H. Lee, C. B. Park, *Adv. Funct. Mater.* **2010**, *20*, 2132.
- [29] S. H. Lee, D. H. Nam, J. H. Kim, J.-O. Baeg, C. B. Park, *ChemBioChem* **2009**, *10*, 1621.
- [30] S. H. Lee, D. H. Nam, C. B. Park, *Adv. Synth. Catal.* **2009**, *351*, 2589.
- [31] C. Oubre, P. J. Nordlander, *Proc. SPIE* **2003**, *5221*, 133.
- [32] N. G. Greeneltch, A. S. Davis, N. A. Valley, F. Casadio, G. C. Schatz, R. P. Van Duyne, N. C. Shah, *J. Phys. Chem. A* **2012**, *116*, 11863.
- [33] S. H. Lee, J. H. Kim, C. B. Park, *Chem. Eur. J.* **2013**, *19*, 4392.
- [34] J. Ryu, S. H. Lee, D. H. Nam, C. B. Park, *Adv. Mater.* **2011**, *23*, 1883.
- [35] J. H. Kim, M. Lee, J. S. Lee, C. B. Park, *Angew. Chem. Int. Ed.* **2012**, *51*, 517.
- [36] Y. Tachibana, L. Vayssieres, J. R. Durrant, *Nat. Photon.* **2012**, *6*, 511.
- [37] J.-D. Rochaix, *Science* **2013**, *342*, 50.
- [38] J. Barber, *Chem. Soc. Rev.* **2009**, *38*, 185.
- [39] R. A. Zangmeister, T. A. Morris, M. J. Tarlov, *Langmuir* **2013**, *29*, 8619.
- [40] M. Ambrico, P. F. Ambrico, A. Cardone, N. F. Della Vecchia, T. Ligonzo, S. R. Cicco, M. M. Talamo, A. Napolitano, V. Augelli, G. M. Farinola, M. d'Ischia, *J. Mater. Chem. C* **2013**, *1*, 1018.
- [41] V. Ball, D. D. Frari, V. Toniazzo, D. Ruch, *J. Colloid Interface Sci.* **2012**, *386*, 366.
- [42] S. D. Standridge, G. C. Schatz, J. T. Hupp, *J. Am. Chem. Soc.* **2009**, *131*, 8407.
- [43] T. Kawawaki, Y. Takahashi, T. Tatsuma, *Nanoscale* **2011**, *3*, 2865.
- [44] L. Duan, M. Chen, S. Zhou, L. Wu, *Langmuir* **2009**, *25*, 3467.
- [45] E. Nitani, S. Miyayama, *Opt. Eng.* **1996**, *35*, 900.
- [46] P. B. Johnson, R. W. Christy, *Phys. Rev. B* **1972**, *6*, 4370.